

Article

The Contribution of Various Plasticity Mechanisms to the Deformation Behavior of Gradient Nanograined FeNi Alloy

Aleksandr V. Korchuganov ^{*}, Konstantin P. Zolnikov and Dmitriy S. Kryzhevich

Institute of Strength Physics and Materials Science of Siberian Branch of Russian Academy of Sciences, Akademicheskii 2/4, 634055 Tomsk, Russia; kost@ispms.ru (K.P.Z.); kryzhev@ispms.ru (D.S.K.)

* Correspondence: avkor@ispms.ru

Abstract: This paper investigates the deformation behavior of a gradient grained FeNi sample under uniaxial tension using molecular dynamics simulations. The simulated sample consists of five layers with grains of the same size in each layer ranging from 10 to 30 nm. It is shown that the sample plasticity develops through sequential activation of different mechanisms. These are either the generation of certain structural defects, or grain boundary migration, or grain boundary sliding. The onset of plasticity is provided by partial dislocations that produce stacking faults in large grains. Other mechanisms involved in plastic deformation are the nucleation of trailing/full dislocations and twinning, which gradually affect smaller and smaller grains. Grain boundary sliding is more intensive in smallest grains due to their less constraint. Grain boundary migration generally leads to the growth of large grains. At strains below 7.0%, plasticity is mainly contributed by the evolution of stacking faults. At higher strains, the main plasticity mechanisms are twinning and grain boundary migration. As the strain increases, the maximum values of accumulated shear, the density of intragranular defects, and the number of atoms involved in intergranular rearrangements are observed first in large, then in medium, and finally in small grains.

Keywords: plasticity mechanism; dislocation; twin; stacking fault; grain boundary migration; grain boundary sliding; molecular dynamics



Citation: Korchuganov, A.V.; Zolnikov, K.P.; Kryzhevich, D.S. The Contribution of Various Plasticity Mechanisms to the Deformation Behavior of Gradient Nanograined FeNi Alloy. *Metals* **2022**, *12*, 573. <https://doi.org/10.3390/met12040573>

Academic Editor: Frank Czerwinski

Received: 21 February 2022

Accepted: 24 March 2022

Published: 28 March 2022

Publisher's Note: MDPI stays neutral with regard to jurisdictional claims in published maps and institutional affiliations.



Copyright: © 2022 by the authors. Licensee MDPI, Basel, Switzerland. This article is an open access article distributed under the terms and conditions of the Creative Commons Attribution (CC BY) license (<https://creativecommons.org/licenses/by/4.0/>).

1. Introduction

Metallic materials combining high strength and ductility are developed using a wide variety of approaches for the creation of heterogeneous and hierarchical structures [1–17]. Among the most advanced heterogeneous materials are gradient grained metallic materials [12–17], in which the grain size usually decreases towards the free surface.

The combination of high strength and ductility in gradient grained materials is achieved due to effective stress redistribution between grains of different sizes in the entire sample volume, which prevents strain localization [18]. Plastic deformation first begins in large grains. At higher loads, plasticity propagates from large grains to smaller ones [19]. Deformed large grains are strengthened due to the accumulation of dislocations and thus contribute to the overall strain hardening of the sample [20]. Small grains are weakened due to grain boundary (GB) migration and coarsening [12,14,16]. This is the way how various mechanisms of plastic deformation are simultaneously activated for strongly different elements of the gradient grained structure. As a result, the fine-grained surface layer of the gradient material, while maintaining the high strength of the entire sample, is able to deform together with other parts of the sample to a much higher strain than a homogeneous fine-grained counterpart.

Studies of gradient grained metallic materials revealed a number of ways to improve their performance characteristics. In [15], it was proposed to create novel metallic materials with high strength and ductility by designing gradient nanotwinned structures through the combination of different-scale structural gradients. According to this approach, a sample

with a gradient grained structure has a gradient in twin boundary spacing. The application of loads to such materials leads to a specific pattern of geometrically necessary dislocations in them, causing plastic strain delocalization and strain hardening.

A transmission electron microscopy study of gradient nanostructured Cu and CuAl samples showed that grain coarsening is the dominant plastic deformation mechanism of nanograins in copper [16]. CuAl samples have a tendency to deformation twinning in nanograins, which increases with increasing Al content. The authors showed that deformation twinning is an effective deformation mechanism that slows down strain localization and enhances nanograin plasticity in tension.

One of the most effective approaches to studying gradient materials is atomistic simulation. It provides detailed information on the generation and evolution of structural defects in single crystal and nanocrystalline metals and alloys [21–25]. For example, a molecular dynamics simulation of nanocrystalline copper showed that the strength of gradient samples correlates with the average grain size and obeys the direct and inverse Hall–Petch relation [26]. For an average grain size of ~10 nm corresponding to the transition from direct to inverse Hall–Petch effect, GB migration and rotations of 7–10-nm grains dominate in the early stages of deformation. As the strain increases, the plastic deformation of the gradient sample is to a greater extent determined by dislocation activity in 12–23-nm grains. An increase in the grain size gradient leads to a decrease in the average critical grain size, below which hardening is replaced by softening, and the Hall–Petch relation breaks down [27]. This effect is associated with simultaneous suppression of GB sliding and GB migration, as well as enhancement of intragranular deformation mechanisms. The coarsening of nanograins in gradient copper during deformation, which leads to softening, strongly depends on the temperature and strain rate [14]. This is due to the fact that nanograin coarsening can be governed by the thermally activated motion of dislocations in deformed grains, rather than by diffusion processes.

Despite significant progress in understanding the deformation behavior of gradient grained materials, little is known about the activation sequences of various plasticity mechanisms in layers with different grain sizes, their interaction, and their contribution to plasticity during loading. In the present work, these issues are investigated by molecular dynamics simulations of a gradient nanograin FeNi sample with an axial grain texture under uniaxial tension.

2. Computational Procedure

Molecular dynamics simulations were carried out using the LAMMPS code [28]. Interatomic interaction in the Fe–Ni system was described by a many-body potential calculated with the embedded atom method [29]. This potential correctly describes the phase diagram of the Fe–Ni system, elastic moduli, and stacking fault energies for a wide range of chemical element concentrations. The simulated sample had the shape of a parallelepiped. Its dimensions along the X, Y and Z axes were 60, 53 and 80 nm, respectively (Figure 1). Periodic boundary conditions were imposed in the X and Y directions; free surfaces were directed along the Z axis. The sample had an equiatomic chemical composition and consisted of grains with the fcc lattice. The grain structure was modeled using the Laguerre–Voronoi tessellation method, with the [123] texture axis parallel to the Y axis for all grains. The misorientation angle between adjacent grains was more than 30 degrees. The gradient grained structure was modeled along the Z axis and consisted of five layers with grains of approximately the same size in each layer. The layers near the free surfaces contained small grains of size 10 nm. Their adjacent layers contained medium-sized grains of 15 nm, and the central layer consisted of large 30-nm grains. The centers of grains of the same size were located in the plane perpendicular to the Z axis at the sites of a conditional triangular lattice.

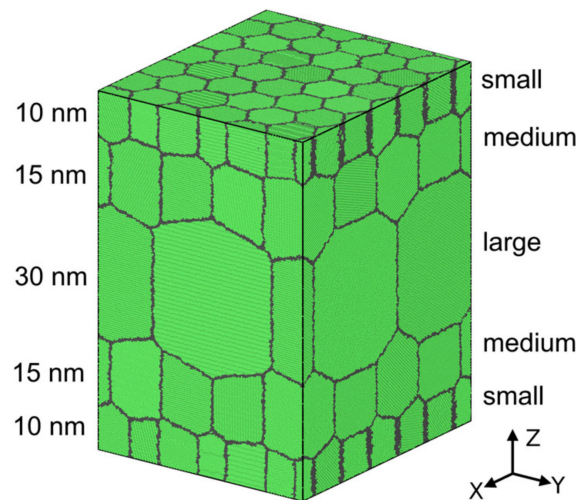


Figure 1. The initial structure of the gradient nanograined FeNi sample. Atoms with fcc nearest neighbor symmetry are highlighted in green; grain boundary (GB) atoms are shown in gray.

The sample was uniformly stretched along the Y axis at a constant rate of 5 m/s by scaling the Y coordinate for all atoms. The relaxation and loading of the sample were performed using a Nose–Hoover thermostat and barostat [30,31] to maintain a temperature of 300 K and zero stress in the X direction.

The accumulated local shear strain was estimated by calculating the displacement parameter constructed on the basis of the slip vector [32]. This parameter for atom i is the sum of the absolute values of the displacements of nearest neighbors relative to this atom at the current time:

$$D_i = \sum_j^n \left| \vec{R}_{ij} - \vec{R}_{ij}^0 \right| \quad (1)$$

where \vec{R}_{ij} and \vec{R}_{ij}^0 are the radius vectors between atoms i and j at the current and initial times, respectively, and n is the number of nearest neighbors of atom i at the current time. Using the displacement parameter, we can identify atoms near which a dislocation passes or a GB migrates.

Structural defects were determined on the basis of common neighbor analysis [33]. Intrinsic stacking faults (ISFs) were identified as two layers of atoms with hcp nearest neighbor symmetry. Twin boundaries were identified as one layer of atoms with hcp nearest neighbor symmetry. The structure of the samples was visualized using the OVITO package [34]. To calculate the spatial density distribution of structural defects in grains, the simulated sample was cut into 1-nm thick slices along the Z direction. Then we counted the number of atoms in each slice which formed a particular structural defect. The resulting number was divided by the total number of atoms in the sample. The shear strain in the layer was estimated by calculating the total displacement parameter D equal to the sum of the displacement parameters of atoms in the given layer.

3. Simulation Results and Discussion

According to the calculations, plastic deformation in the simulated sample begins at ~2.9% tensile strain. The main plasticity mechanism up to ~3.0% strain is the generation of ISFs. First, partial dislocations are formed at the boundaries of large grains and propagate into their bulk to form first ISFs. As the tensile strain increases, ISFs begin to form in medium and small grains. The calculation results are consistent with experimental observations [19] where the onset of plasticity in gradient grained samples was found to be due to the formation of dislocations in coarse grains.

Up to $\sim 3.7\%$ strain, ISFs are most actively formed in large grains (Figures 2a and 3a,b). At a strain above $\sim 4.1\%$, there begins an intense emission of trailing dislocations at the boundaries of large grains which remove ISFs from these grains. This process is accompanied by the activation of the twinning mechanism occurring through the transformation of part of the ISFs into twins. As a result, the ISF density decreases within the 4.1–4.5% strain range (Figure 3b), while the twin density increases (Figure 3c–f). The accumulated shear strain in large grains at 4.1% strain and above exceeds that for grains of other sizes (Figure 4). This is due to the more active generation of trailing dislocations and twins in the coarse-grained layer compared to other layers, as a result of which stresses in large grains are significantly relaxed. Note that although the accumulated shear strain in large grains is higher above a strain of 3.7%, the defect density is much higher in medium and small grains (Figures 2b and 3a). This is due to the fact that ISFs that continue to form in large grains are removed by trailing dislocations. In medium and small grains, trailing dislocations are less readily formed than leading ones due to the smaller size of these grains compared to large grains [35].

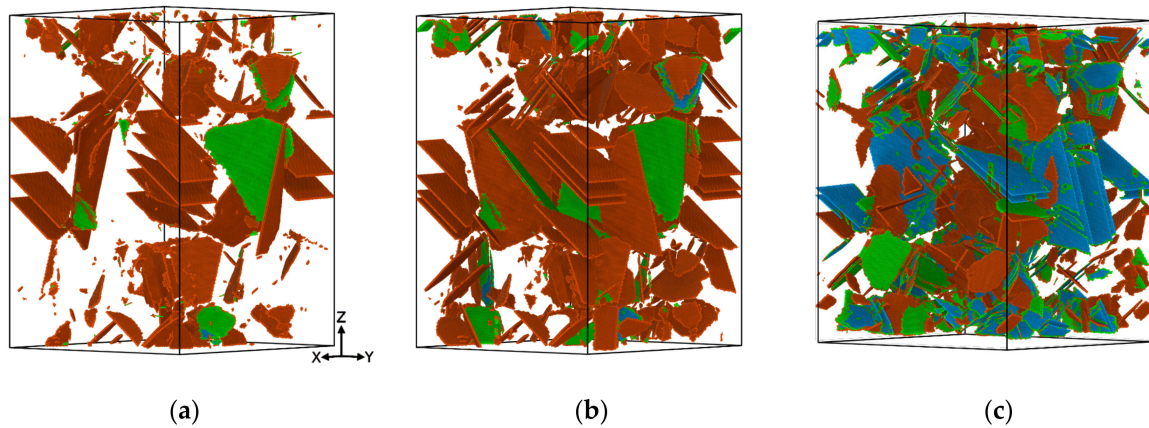


Figure 2. Structural defects in the sample strained to: (a) 3.7, (b) 4.5, and (c) 20.0%. Intrinsic stacking faults (ISFs) and twin boundaries with a thickness of one or more atomic planes are highlighted in red, green and blue, respectively.

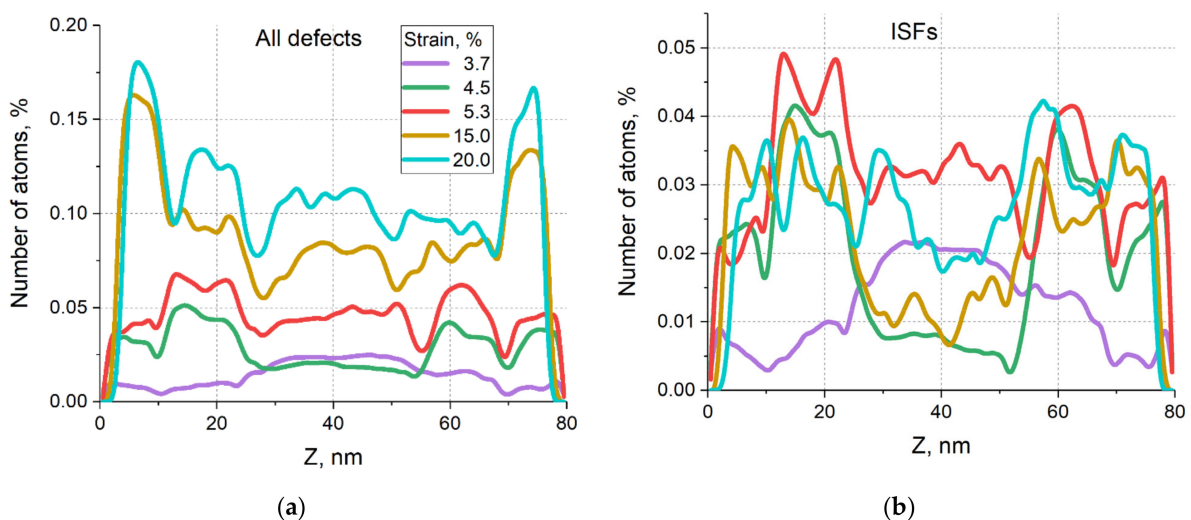


Figure 3. Cont.

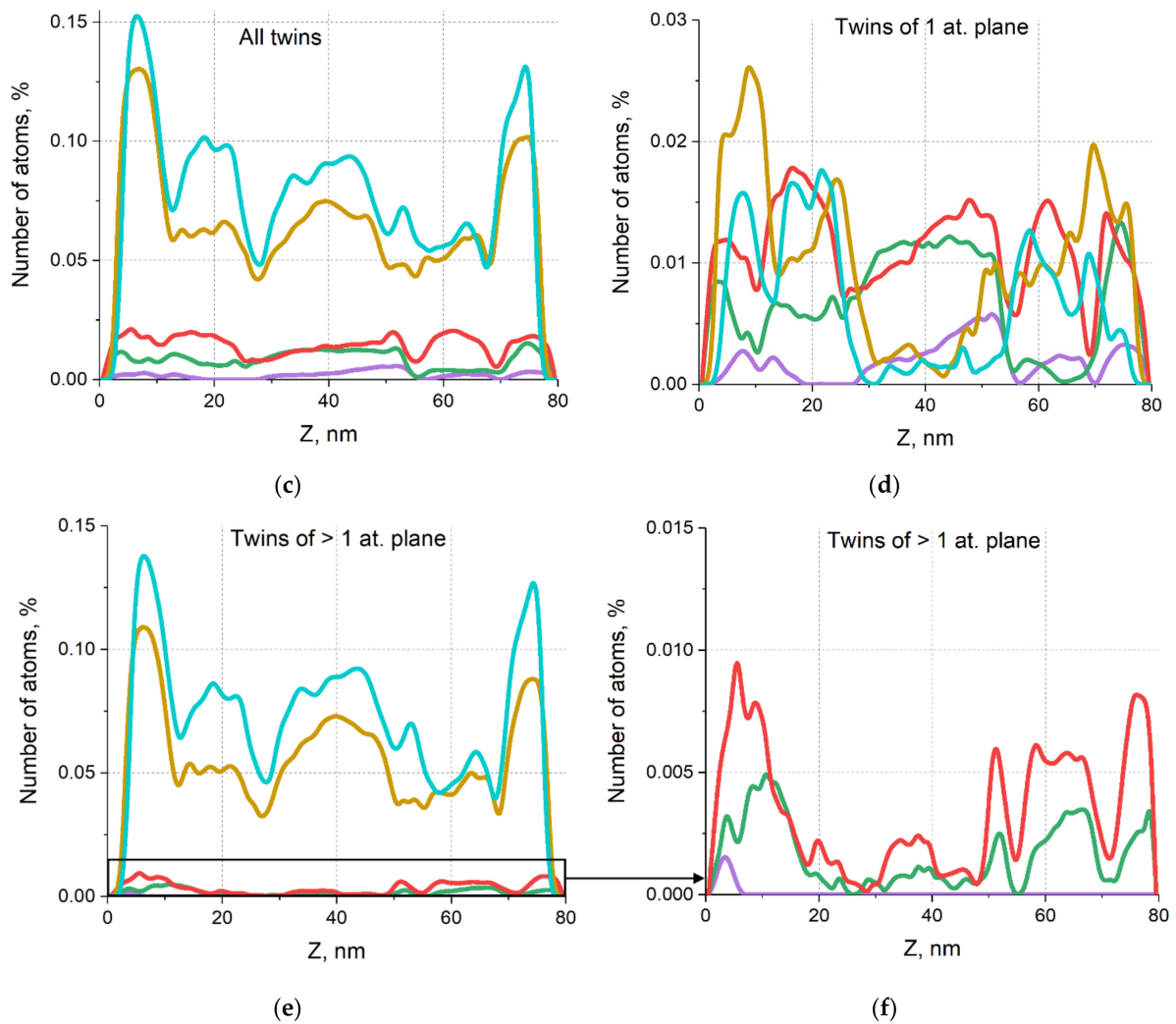


Figure 3. Z-axial distribution of the fraction of atoms constituting: (a) all defects, (b) ISFs, (c) twins, (d) twins with a thickness of 1 atomic plane, (e,f) twins with a thickness of more than 1 atomic plane for different strains.

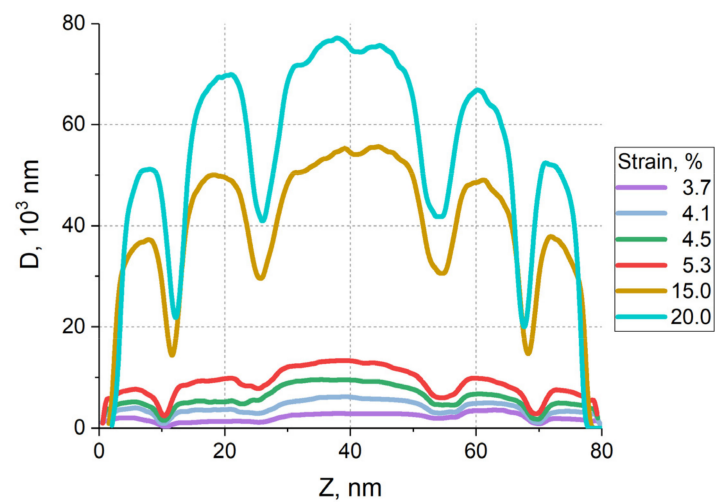


Figure 4. Z-axial distribution of the total displacement parameter D in grains for different tensile strains in the sample.

In the strain range from 4.5 to 5.3%, shear deformation in grains of all sizes increases at approximately the same rate (Figure 4), the number of defects increases, and the maximum density of all defects is observed for medium grains (Figure 3a). The ISF density in large grains increases again (Figure 3b), while in small and medium grains it remains virtually unchanged. Figure 3c shows that up to a strain of 5.3% twins are relatively uniformly distributed over the sample volume. Twins with one fcc atomic plane between their boundaries are seen to rapidly form in small and medium grains in the given strain range (Figure 3d). Twins in grains of all sizes are still formed from existing ISFs (Figure 5). The nucleation and motion of twinning dislocations in the slip planes adjacent to ISFs cause the transformation of the ISFs (shown in red in Figures 2 and 5) into twins with one fcc layer thickness (green in Figures 2 and 5). These twins are then transformed by subsequent twinning dislocations into twins with more than one fcc layer thickness (blue in Figures 2 and 5). The dynamics of changes in the number of atoms that make up twins of different thicknesses with increasing strain is shown in Figure 3d–f. One can see that twins of different thicknesses are distributed differently along the structural gradient. As the strain increases, twins with more than one atomic plane thickness tend to accumulate faster in small grains. The maximum twin density is first observed in large grains, then in medium, and finally in small grains.

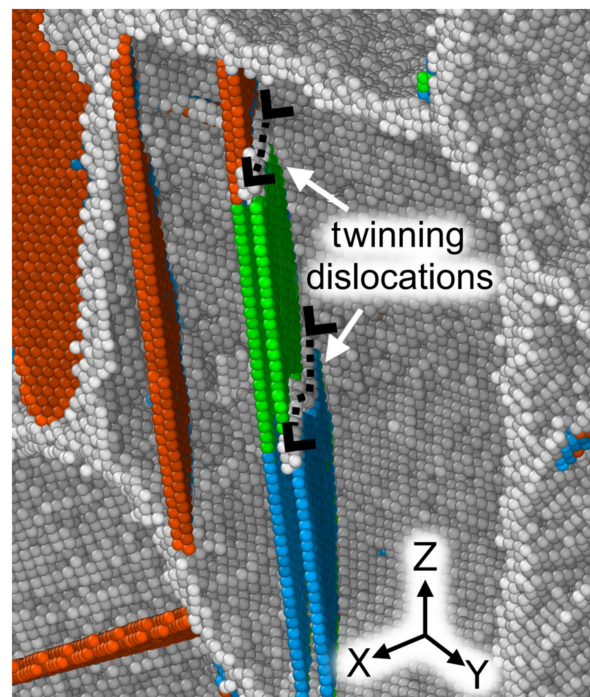


Figure 5. Transformation of ISF into a twin in a medium grain. ISFs are shown in red, boundaries of twin with one atomic plane thickness are green, boundaries of twin with more than one atomic plane thickness are blue, and atoms with uncertain nearest neighbor symmetry (GBs and dislocations) are gray. Atoms with fcc nearest neighbor symmetry are not shown.

The calculation results showed that the major part of plastically deformed material (the number of atoms constituting structural defects) in large grains up to 6.0% strain is related to the evolution of ISFs in them. In medium and small grains, plasticity is mainly contributed by partial dislocations up to 6.5–7.0% strains.

It should be noted that nanocrystalline materials have a high density of GBs that contribute to plasticity either indirectly through dislocation emission from their regions, or directly through such grain boundary plasticity mechanisms as GB migration and GB sliding. GB migration occurs at a tensile strain of ~4.0% in the entire sample volume. Its contribution to plasticity increases faster for smaller grains. As a rule, GB migration leads to

the growth of larger grains at the expense of smaller ones (Figure 6). However, the direction and magnitude of GB displacements in each case are determined by the stress distribution in the GB region, the degree of nonequilibrium of the GB and triple junctions, and the distribution of structural defects in adjacent grains. GB migration is inhomogeneous over the sample cross section due to coarsening of the grains that are located in the stress concentration zones and are favorably oriented. Analysis of the simulation results showed that GB migration and twinning become the main plasticity mechanisms in grains above ~ 7.0 – 7.5% tensile strains. In this case, the contribution of GB migration to the volume fraction of plastically deformed material exceeds that of twinning. This is consistent with experimental observations [36,37], which note that the GB activity is the main plasticity mechanism of the FeNi nanocrystalline alloy with an average grain size of 12–33 nm.

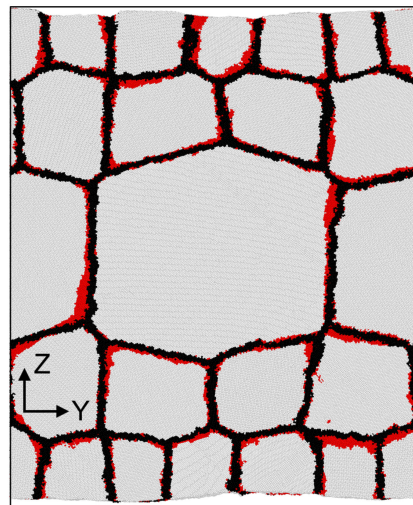


Figure 6. GB displacements for the sample cross section at $X = 24$ nm. GB atoms at 0% deformation are shown in black. Atoms involved in GB displacements during stretching to 20% are in red.

Figure 7 shows the largest GB displacement in the deformed sample. This migration led to coarsening of the upper grain at the expense of the lower larger grain. A dislocation wall formed near the triple junction of these grains and separated a fragment from the upper grain (bounded by the dotted line in Figure 7) which has a lattice orientation different from that of the adjacent grains. The figure shows the change in the position of the considered GB during sample stretching. The position of the GB triple junctions practically did not change and they restrained the GB migration.

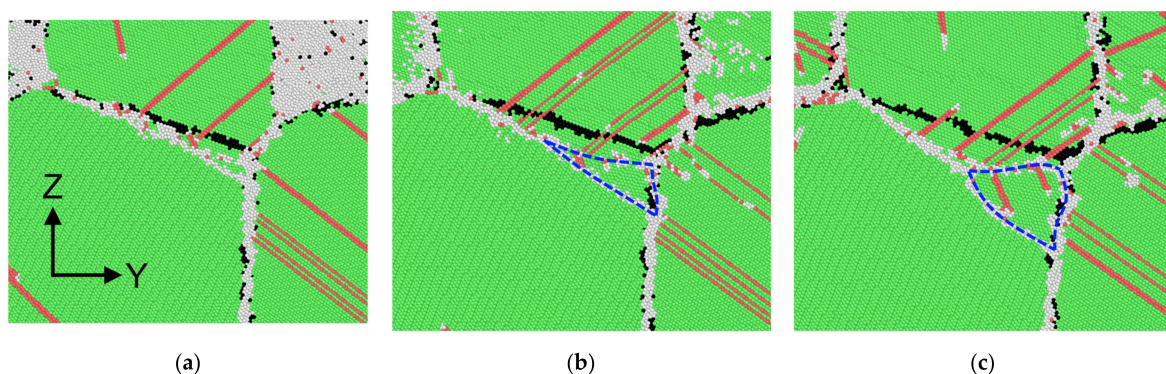


Figure 7. GB migration between a large and a medium grain. A cross-section fragment of the sample at $X = 10$ nm for strains: (a) 5.3, (b) 10.0, and (c) 15.0%. Atoms with fcc, hcp, and uncertain nearest neighbor symmetry are colored green, red, and gray, respectively. GB atoms at 0% strain are shown in black.

The role of GB sliding in the accommodation of the material structure increases with increasing strain. This mechanism is most pronounced in the layers with small grains as they have the maximum density of GBs (Figure 8a). Owing to the higher strength and less constraint (adjoining to the free surface), small grains can slide along GBs as a whole. The change in the amount of strain-induced GB sliding for several GB regions marked with circles in Figure 8a is shown in Figure 8b. It can be seen that slip is strongly activated at ~4.0% tensile strain for all indicated grains. All of the curves presented in Figure 8b have deformation intervals with fast GB sliding and intervals with slow or even zero slip. Slipping slows down or stops due to the emission of structural defects from GBs and triple junctions, leading to stress relaxation in the GB region. For example, at strains of 11.5 and 14.5% ISFs are emitted from the GB in region 3; at 7.0% strain a twin in a small grain begins to grow in region 6. These results are in good agreement with theoretical models of the accommodation mechanisms of GB sliding [38,39]. The cited studies showed that the accommodation of GB sliding can be associated with the emission of dislocations from GBs and their junctions, as well as with the cooperative GB migration or nucleation of new grains in triple junctions. We have found that grains can slip due to intragranular shear in their neighbors. Figure 9 demonstrates that the region of large grain I marked by a dotted line is sheared by dislocations and twins. The adjacent medium grain II is displaced as a whole and slips along the boundary with grain III. In so doing, a part of medium grain III slips along the boundary with grain IV towards the displaced grain II. The behavior of the simulated sample is consistent with the conclusion from [12] that with increasing strain the dominant role in the development of plasticity passes from dislocation glide to intergranular processes, which are enhanced with decreasing grain size.

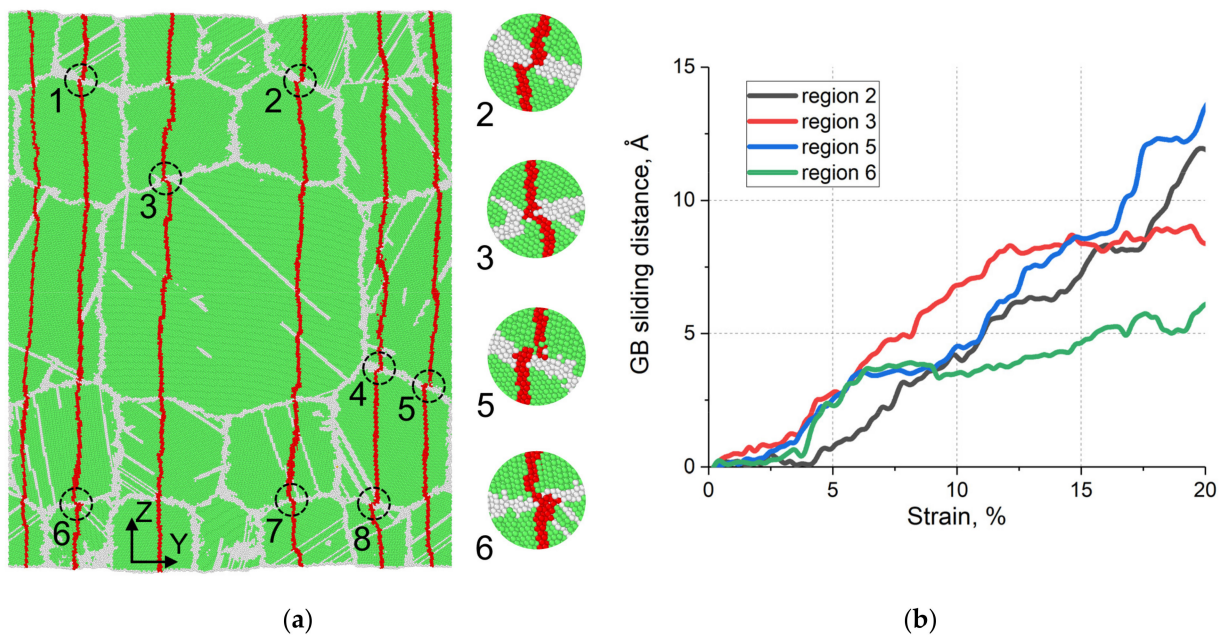


Figure 8. (a) Sample cross section at X = 40 nm for strain 15.0% showing the result of GB sliding. Atoms with fcc nearest neighbor symmetry are highlighted in green. Atoms located on straight lines at 0% strain are red. Atoms belonging to GBs and structural defects are light gray. (b) GB sliding distance vs. strain in the regions circled in Figure (a).

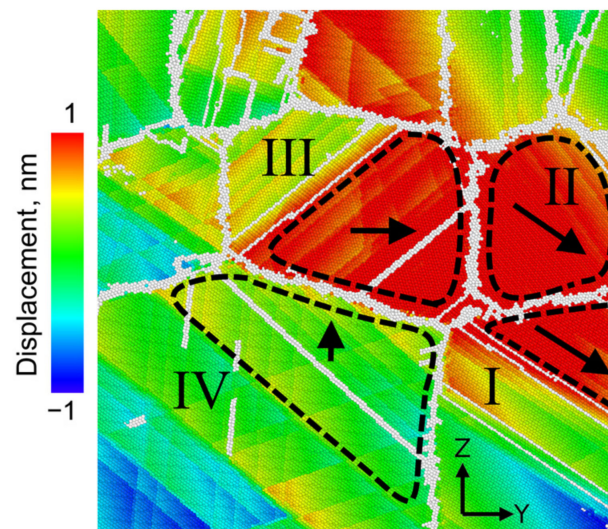


Figure 9. GB sliding pattern in a sample fragment in the cross section at $X = 49$ nm for strain 15.0%. The arrows indicate the scaled average displacement vectors for the outlined areas. Atoms are colored according to the Y component of their displacement. Atoms belonging to GBs and structural defects are marked in light gray.

Starting from a strain of $\sim 7.0\%$, the defect density increases faster in small grains than in other grains. At 15.0% strain, it significantly exceeds the defect density in medium and large grains (Figure 3a). The ISF density in small and medium grains is approximately the same and is much higher than in large grains (Figure 3b). The maximum density of defects in small grains was reached primarily due to the large number of twins with more than one atomic plane thickness (Figure 3f). It was found that at high strains there are no twin nuclei in large grains, but they are formed only in medium and small grains. Consequently, the formation of ISFs and twins is more intense in these grains. Plasticity in large grains develops due to an increase in the thickness of existing twins and intense slip of full dislocations. The distribution curve of the displacement parameter shows that at strains above 4.1% the larger the grain size, the greater the cumulative shear (Figure 4). This is due to the fact that the development of plasticity in the layer with small grains is largely determined by intergranular mechanisms. In the strain range from 15 to 20%, the density of twins increases in all grains, and the density of ISFs again increases significantly in large grains (Figure 3b,c). The accumulated shear in large grains remains maximum due to intense twinning and motion of full dislocations (Figure 4a).

One of the loading parameters that greatly affect the mechanisms of plasticity is the strain rate. We studied the behavior of the simulated sample under uniaxial tension at a rate of 0.5 m/s. The loading scheme and the initial temperature were the same as in the above calculations. It was found that structural defects begin to form at a lower strain ($\sim 2.5\%$), and the plastic flow stress of the material is approximately 5% lower than that at a rate of 5 m/s. This material behavior is due to the longer time of sample structure accommodation to the applied load with decreasing strain rate. A longer structure accommodation time leads to greater dislocation activity in the deformed sample. Calculation results for the total displacement parameter at high strains (15%) showed that it increases by 9.0% in grains and by 15.0% in GBs compared to the results of loading at a rate of 5.0 m/s. The contribution of the two main plasticity mechanisms (twinning and GB migration) to the structural transformation of the material during tension is represented in Figure 10. The number of atoms that form twins at a tension rate of 0.5 m/s at strains above 7.0% is smaller than in tension at a rate of 5.0 m/s (Figure 10a). This agrees with the experimental data showing that twinning is activated as the strain rate increases [40]. A decrease in the contribution of twinning to material plasticity at a lower tension rate occurs in parallel with increasing dislocation activity, leading to a more efficient relaxation of internal stresses. GB

migration is intensified with decreasing strain rate (Figure 10b) due to an increase in the time of structure accommodation to the applied load. In this case, the material volume involved in GB migration at a lower strain rate is much larger than that at a rate of 5.0 m/s.

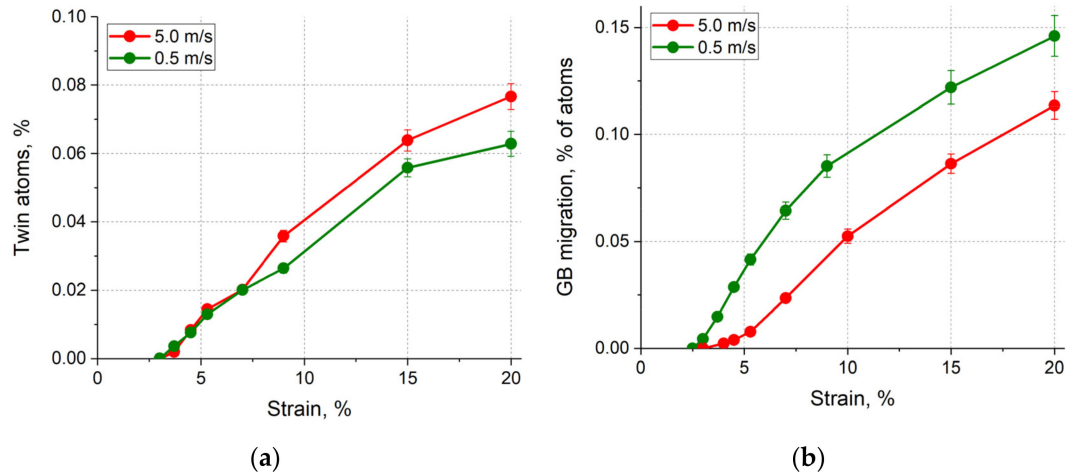


Figure 10. Strain dependence of the number of atoms forming twins (a) and the number of atoms through which GBs migrated (b) for two strain rates.

The qualitative picture of plasticity development in layers with different grain sizes is illustrated in the deformation map in Figure 11. The color saturation on this map of plasticity mechanisms corresponds to the number of atoms involved in the formation and motion of various defects (leading and trailing partial dislocations, full dislocations, twins), or the number of atoms by which the grain sizes changed due to GB migration.

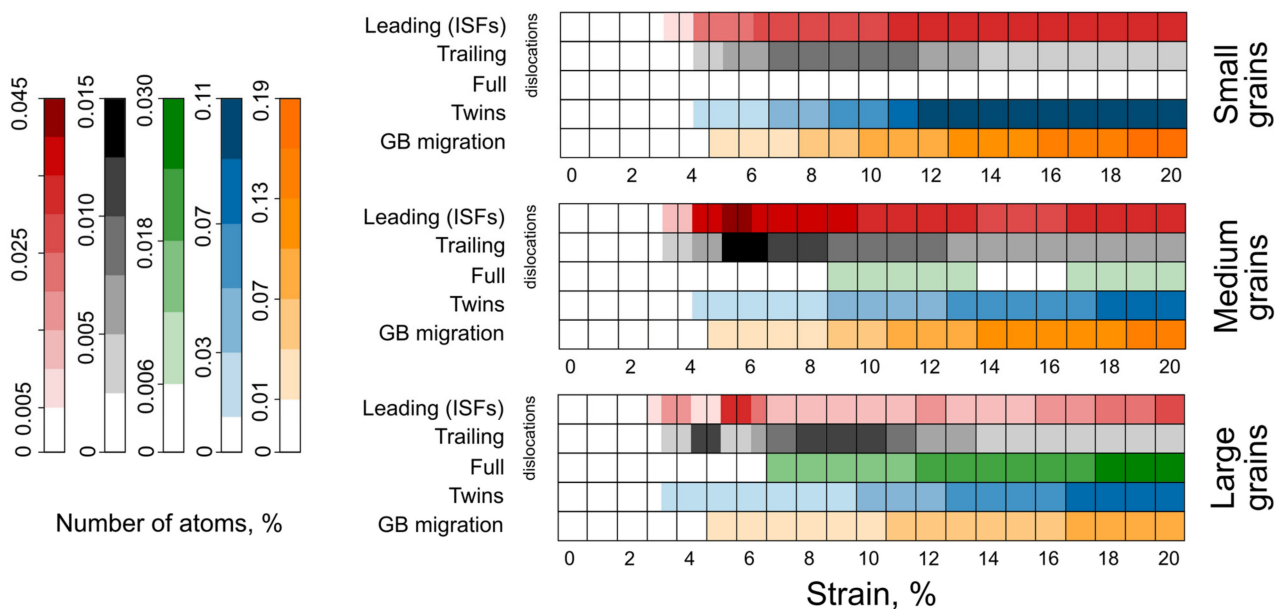


Figure 11. Deformation map showing the contribution of various mechanisms to plasticity development in different-sized grains of a deformed gradient nanograined sample.

It can be seen from the map that the onset of plasticity occurs sequentially in large, medium, and then small grains through partial dislocations. Twinning and GB migration constantly increase their contribution in all sample layers with increasing strain and begin to dominate over other mechanisms above a strain of 7–10%. The contribution from

dislocation slip can change with strain since the map shows only the current density of defects of this type. In this case, the number of emitted dislocations constantly grows, increasing the contribution of dislocations to the total shear strain of the sample. Note that the deformation map does not show the contribution from GB sliding as it cannot be expressed in terms of the number of atoms. Almost all atoms belonging to GBs participate in GB sliding, but they are displaced by different distances even in one GB.

4. Conclusions

The molecular dynamics study of the deformation behavior of a gradient nanograined FeNi sample revealed a sequential involvement of different mechanisms in plastic deformation. These mechanisms contribute to material plasticity through intergranular rearrangements, generation of various structural defects in grains, and their consistent evolution in layers with different grain sizes.

The role of the GB sliding in the material behavior constantly increases with increasing strain. This mechanism is most intense in layers with small grains due to their less constraint, greater strength, and the highest GB density in these layers. At ~2.9% strain, the formation of ISFs begins in large grains as a result of the emission of partial dislocations from GBs and their subsequent propagation.

At ~4.1% strain, part of the ISFs formed in large grains is removed by trailing dislocations, and some ISFs are transformed into twins as a result of partial dislocation slip in the slip plane adjacent to the ISFs. These processes lead to the most pronounced increase in the accumulated shear strain and significant stress relaxation in large grains. Then, plastic shearing begins in small grains and the density of ISFs in them becomes higher than in large grains. At strains above 4.1%, the total accumulated shear strain is higher in large grains.

The contribution of twinning to plasticity increases with increasing strain successively from large to small grains, and the maximum twin density in the sample sequentially shifts from large to medium and then to small grains. However, the greatest contribution to material plasticity up to ~7.0% strain is governed by the evolution of ISFs. Above 7.0%, full dislocations begin to form in medium and large grains.

Another important plasticity mechanism activated at ~4.0% tensile strain is GB migration. As a rule, GB migration leads to the growth of large grains at the expense of small grains. At strains above 7.0%, twinning and GB migration become the main plasticity mechanisms in grains. The contribution of GB migration to the volume fraction of plastically deformed material exceeds the contribution from twinning.

As the tension rate decreases, the contributions of GB migration and dislocation processes to material plasticity increase, while the contribution of twinning decreases. Such changes in the mechanisms of plasticity are primarily due to an increase in the time of sample structure accommodation to the applied load.

The simulation results were analyzed and used to construct a deformation map that clearly illustrates the sequence and intensity of the main plasticity mechanisms in the simulated gradient nanograined FeNi sample, as well as the volume of plastically deformed material in layers with different grain sizes during loading.

Author Contributions: Conceptualization and methodology, A.V.K. and K.P.Z.; validation and investigation, A.V.K. and D.S.K.; writing—original draft preparation, A.V.K.; writing—review and editing, A.V.K., K.P.Z. and D.S.K.; software—D.S.K.; visualization, A.V.K.; supervision and project administration, A.V.K. All authors have read and agreed to the published version of the manuscript.

Funding: Investigation of the plastic deformation mechanisms and their contribution to material plasticity was carried out with the financial support of the Russian Science Foundation (Project No. 20-79-10406). The effect of strain rate on the evolution of the defect structure was studied under the government statement of work for ISPMS SB RAS (Project FWRW-2021-0002).

Data Availability Statement: Not applicable.

Conflicts of Interest: The authors declare no conflict of interest.

References

1. Ovid'ko, I.A.; Valiev, R.Z.; Zhu, Y.T. Review on superior strength and enhanced ductility of metallic nanomaterials. *Prog. Mater. Sci.* **2018**, *94*, 462–540. [[CrossRef](#)]
2. Ma, Y.; Yang, M.; Yuan, F.; Wu, X. A review on heterogeneous nanostructures: A strategy for superior mechanical properties in metals. *Metals* **2019**, *9*, 598. [[CrossRef](#)]
3. Ma, E.; Zhu, T. Towards strength–ductility synergy through the design of heterogeneous nanostructures in metals. *Mater. Today* **2017**, *20*, 323–331. [[CrossRef](#)]
4. Lu, K. Stabilizing nanostructures in metals using grain and twin boundary architectures. *Nat. Rev. Mater.* **2016**, *1*, 16019. [[CrossRef](#)]
5. Jin, K.; Zhang, C.; Zhang, F.; Bei, H. Influence of compositional complexity on interdiffusion in Ni-containing concentrated solid-solution alloys. *Mater. Res. Lett.* **2018**, *6*, 293–299. [[CrossRef](#)]
6. Xu, T.; Wang, S.; Wang, W.; Liang, P.; Li, X.; Mitsuzaki, N.; Chen, Z. Multimodal grain structure and tensile properties of cold-rolled titanium after short-duration annealing. *Mater. Charact.* **2020**, *160*, 110095. [[CrossRef](#)]
7. Li, Z.; Pradeep, K.G.; Deng, Y.; Raabe, D.; Tسان, C.C. Metastable high-entropy dual-phase alloys overcome the strength-ductility trade-off. *Nature* **2016**, *534*, 227–230. [[CrossRef](#)]
8. Li, J.; Lu, W.; Chen, S.; Liu, C. Revealing extra strengthening and strain hardening in heterogeneous two-phase nanostructures. *Int. J. Plast.* **2019**, *126*, 102626. [[CrossRef](#)]
9. Sun, L.; He, X.; Lu, J. Nanotwinned and hierarchical nanotwinned metals: A review of experimental, computational and theoretical efforts. *NPJ Comput. Mater.* **2018**, *4*, 6. [[CrossRef](#)]
10. Wu, X.; Yang, M.; Yuan, F.; Wu, G.; Wei, Y.; Huang, X.; Zhu, Y. Heterogeneous lamella structure unites ultrafine-grain strength with coarse-grain ductility. *Proc. Natl. Acad. Sci. USA* **2015**, *112*, 14501–14505. [[CrossRef](#)]
11. Wang, Y.F.; Wang, M.S.; Fang, X.T.; Guo, F.J.; Liu, H.Q.; Scattergood, R.O.; Huang, C.X.; Zhu, Y.T. Extra strengthening in a coarse/ultrafine grained laminate: Role of gradient interfaces. *Int. J. Plast.* **2019**, *123*, 196–207. [[CrossRef](#)]
12. Lu, K. Making strong nanomaterials ductile with gradients. *Science* **2014**, *345*, 1455–1456. [[CrossRef](#)] [[PubMed](#)]
13. Cao, S.C.; Liu, J.; Zhu, L.; Li, L.; Dao, M.; Lu, J.; Ritchie, R.O. Nature-Inspired Hierarchical Steels. *Sci. Rep.* **2018**, *8*, 5088. [[CrossRef](#)] [[PubMed](#)]
14. Chen, W.; You, Z.S.; Tao, N.R.; Jin, Z.H.; Lu, L. Mechanically-induced grain coarsening in gradient nano-grained copper. *Acta Mater.* **2017**, *125*, 255–264. [[CrossRef](#)]
15. Cheng, Z.; Zhou, H.; Lu, Q.; Gao, H.; Lu, L. Extra strengthening and work hardening in gradient nanotwinned metals. *Science* **2018**, *362*, eaau1925. [[CrossRef](#)]
16. Wang, J.J.; Tao, N.R.; Lu, K. Revealing the deformation mechanisms of nanograins in gradient nanostructured Cu and CuAl alloys under tension. *Acta Mater.* **2019**, *180*, 231–242. [[CrossRef](#)]
17. Cao, R.; Yu, Q.; Pan, J.; Lin, Y.; Sweet, A.; Li, Y.; Ritchie, R.O. On the exceptional damage-tolerance of gradient metallic materials. *Mater. Today* **2020**, *32*, 94–107. [[CrossRef](#)]
18. Fang, T.H.; Li, W.L.; Tao, N.R.; Lu, K. Revealing extraordinary intrinsic tensile plasticity in gradient nano-grained copper. *Science* **2011**, *331*, 1587–1590. [[CrossRef](#)]
19. Yang, X.; Ma, X.; Moering, J.; Zhou, H.; Wang, W.; Gong, Y.; Tao, J.; Zhu, Y.; Zhu, X. Influence of gradient structure volume fraction on the mechanical properties of pure copper. *Mater. Sci. Eng. A* **2015**, *645*, 280–285. [[CrossRef](#)]
20. Wu, X.; Jiang, P.; Chen, L.; Yuan, F.; Zhu, Y.T. Extraordinary strain hardening by gradient structure. *Proc. Natl. Acad. Sci. USA* **2014**, *111*, 7197–7201. [[CrossRef](#)]
21. Nikonov, A.Y.; Dmitriev, A.I.; Lychagin, D.V.; Lychagina, L.L.; Bibko, A.A.; Novitskaya, O.S. Numerical study and experimental validation of deformation of <111> fcc CuAl single crystal obtained by additive manufacturing. *Metals* **2021**, *11*, 582. [[CrossRef](#)]
22. Nikonov, A.Y.; Lychagin, D.V.; Bibko, A.A.; Novitskaya, O.S. Growth and Deformation Simulation of Aluminum Bronze Grains Produced by Electron Beam Additive Manufacturing. *Metals* **2022**, *12*, 114. [[CrossRef](#)]
23. Zolnikov, K.P.; Korchuganov, A.V.; Kryzhevich, D.S. Anisotropy of plasticity and structural transformations under uniaxial tension of iron crystallites. *Comput. Mater. Sci.* **2018**, *155*, 312–319. [[CrossRef](#)]
24. Zolnikov, K.P.; Kryzhevich, D.S.; Korchuganov, A.V. Nucleation of Plasticity in Alpha-Iron Nanowires. *Russ. Phys. J.* **2020**, *63*, 947–953. [[CrossRef](#)]
25. Zolnikov, K.P.; Kryzhevich, D.S.; Korchuganov, A.V. Structural Transformations in the Grain Boundary Region of Nanocrystalline Metals Under Mechanical Loading. *Russ. Phys. J.* **2019**, *62*, 1357–1362. [[CrossRef](#)]
26. Sun, J.; Ye, H.; Tao, J.; Li, Q.; Zhang, J.; Shen, L.; Zheng, Y.; Zhang, H. Gradient structure regulated plastic deformation mechanisms in polycrystalline nanotwinned copper. *J. Phys. D Appl. Phys.* **2019**, *52*, 365304. [[CrossRef](#)]
27. Cao, P. The Strongest Size in Gradient Nanograined Metals. *Nano Lett.* **2020**, *20*, 1440–1446. [[CrossRef](#)]
28. Plimpton, S. Fast Parallel Algorithms for Short-Range Molecular Dynamics. *J. Comput. Phys.* **1995**, *117*, 1–19. [[CrossRef](#)]
29. Zhou, X.W.; Foster, M.E.; Sills, R.B. An Fe-Ni-Cr embedded atom method potential for austenitic and ferritic systems. *J. Comput. Chem.* **2018**, *39*, 2420–2431. [[CrossRef](#)]
30. Hoover, W.G. Canonical dynamics: Equilibrium phase-space distributions. *Phys. Rev. A* **1985**, *31*, 1695–1697. [[CrossRef](#)]
31. Martyna, G.J.; Tobias, D.J.; Klein, M.L. Constant pressure molecular dynamics algorithms. *J. Chem. Phys.* **1994**, *101*, 4177–4189. [[CrossRef](#)]

32. Zimmerman, J.A.; Kelchner, C.L.; Klein, P.A.; Hamilton, J.C.; Foiles, S.M. Surface step effects on nanoindentation. *Phys. Rev. Lett.* **2001**, *87*, 165507. [[CrossRef](#)] [[PubMed](#)]
33. Honeycutt, J.D.; Andersen, H.C. Molecular dynamics study of melting and freezing of small Lennard-Jones clusters. *J. Phys. Chem.* **1987**, *91*, 4950–4963. [[CrossRef](#)]
34. Stukowski, A. Visualization and analysis of atomistic simulation data with OVITO—the Open Visualization Tool. *Model. Simul. Mater. Sci. Eng.* **2010**, *18*, 015012. [[CrossRef](#)]
35. Shu, X.; Kong, D.; Lu, Y.; Long, H.; Sun, S.; Sha, X.; Zhou, H.; Chen, Y.; Mao, S.; Liu, Y. Size effect on the deformation mechanisms of nanocrystalline platinum thin films. *Sci. Rep.* **2017**, *7*, 13264. [[CrossRef](#)]
36. Matsui, I.; Mori, H.; Kawakatsu, T.; Takigawa, Y.; Uesugi, T.; Higashi, K. Mechanical behavior of electrodeposited bulk nanocrystalline Fe-Ni alloys. *Mater. Res.* **2015**, *18*, 95–100. [[CrossRef](#)]
37. Li, X.; You, Y.; Yue, Y.; Wu, H. Effect of Current Density on the Microstructure and Mechanical Properties of Bulk NC Ni-Fe Alloy. *Integr. Ferroelectr.* **2013**, *144*, 91–100. [[CrossRef](#)]
38. Bobylev, S.V.; Morozov, N.F.; Ovid'ko, I.A. Cooperative grain boundary sliding and migration process in nanocrystalline solids. *Phys. Rev. Lett.* **2010**, *105*, 055504. [[CrossRef](#)]
39. Bobylev, S.V.; Morozov, N.F.; Ovid'ko, I.A. Cooperative grain boundary sliding and nanograin nucleation process in nanocrystalline, ultrafine-grained, and polycrystalline solids. *Phys. Rev. B—Condens. Matter Mater. Phys.* **2011**, *84*, 094103. [[CrossRef](#)]
40. Rusty Gray, G.T. High-strain-rate deformation: Mechanical behavior and deformation substructures induced. *Annu. Rev. Mater. Res.* **2012**, *42*, 285–303. [[CrossRef](#)]